Chemical Engineering Science 139 (2016) 241–248

Contents lists available at ScienceDirect

Chemical Engineering Science

journal homepage: www.elsevier.com/locate/ces

Two-phase flow with capillary valve effect in porous media

Rui Wu [a,b,*], Abdolreza Kharaghani [a], Evangelos Tsotsas [a]

[a] Chair of Thermal Process Engineering, Otto von Guericke University, P.O. 4120, 39106 Magdeburg, Germany
[b] School of Energy and Power Engineering, University of Shanghai for Science and Technology, Shanghai, 200093, China

HIGHLIGHTS

- Pore network model with the capillary valve effect (CVE) is developed.
- Two types of pore invasion are proposed.
- Simulation and experimental results agree well if CVE is considered.

ARTICLE INFO

Article history:
Received 18 April 2015
Received in revised form
30 August 2015
Accepted 23 September 2015
Available online 9 October 2015

Keywords:
Capillary valve effect
Pore network model
Two-phase flow
Capillary force
Burst invasion
Merge invasion

ABSTRACT

The capillary valve effect is studied on the capillary force dominated immiscible two-phase flows in the networks composed of regular pores and throats. Two types of pore invasion are revealed. One is bursting invasion, where the invading fluid enters a pore from one throat. The other is merging invasion, where a pore is invaded by the invading fluid from two throats. Drainage and imbibition are similar and show capillary fingering pattern in the cases where bursting invasion dominates over merging invasion. When merging invasion is dominant, a stable flow pattern can also be observed.

1. Introduction

Immiscible two-phase flow in porous media is of great interest to many industrial fields, such as oil recovery, CO_2 sequestration, and water management in fuel cells. Nevertheless, it is a challenge to fully understand the two-phase flow in a porous material, since it is affected not only by interactions between gravitational, capillary, and viscous forces but also by the structure of the pore space.

Porous materials contain pores of various sizes, such that small pores may be connected to large pores with a sudden geometrical expansion at their interfaces. This expansion can increase the resistance to the advancement of the invading fluid and has already been employed as a capillary valve to control the fluid flow in microfluidic devices (Duffy et al., 1999; Cho et al., 2007; Chen et al., 2008; Moore et al., 2011). When the invading fluid reaches an expansion interface, it will stop moving until its pressure increases to a critical value. We call this as the capillary valve effect.

Pore network models have been commonly used to understand the two-phase flows in porous media (Blunt, 2001; Sahimi, 2011; Joekar-Niasar and Hassanizadeh, 2012). In this method, the void space of a porous medium is conceptualized as a pore network composed of regular ducts of various sizes. The two-phase flow in a network is depicted by the prescribed rules. In the cases where the capillary forces dominate, the invasion percolation algorithm proposed by Wilkiinson and Willemsen (1983) has been widely used (Blunt et al., 1992; Knackstedt et al., 1998, 2001; Mani and Mohanty, 1999; Lopez and Vidales et al., 2003; Araujo et al., 2005; Bazylak et al., 2008; Chapuis et al., 2008; Rebai and Prat, 2009; Wu et al., 2010, 2012, 2013; Ceballos et al., 2011; Ceballos and Prat, 2013).

Only one network duct is invaded at each step in the invasion percolation algorithm. This duct is the largest available one in drainage, whereas in imbibition, it is the smallest available one. Bazylak et al. (2008) compared the pore network simulations against the experiments for slow drainage in networks of various structures. Differences between them were always observed and attributed to the uncertainty in the network fabrication. Although

* Corresponding author at: Chair of Thermal Process Engineering, Otto von Guericke University, P.O. 4120, 39106 Magdeburg, Germany. Tel.: +49 391 52280; fax: +49 391 11160.
E-mail address: ruiwu1986@gmail.com (R. Wu).

http://dx.doi.org/10.1016/j.ces.2015.09.028
0009-2509/

this is an important reason, it will be shown later that neglecting the capillary valve effect in the pore network model can be another reason.

A pore network model with the capillary valve effect is developed in this paper for simulations of the capillary force dominated two-phase flows in porous media. Experiments for gas–liquid two-phase flows in microfluidic networks are performed. The numerical results agree well with the experimental data if the capillary valve effect is considered in the model. If this effect is not considered, the agreement is not so good.

The paper is organized as follows: In Section 2, the experiments for the gas–liquid two-phase flow in microfluidic networks are depicted. The pore network model with the capillary valve effect is developed in Section 3. In Section 4, the numerical results are compared with the experimental observations. The conclusions are drawn in Section 5.

2. Experiments with microfluidic networks

The gas–liquid two-phase flow experiments are conducted with the microfluidic networks supplied by CapitalBio Corporation (China). The transparent networks are fabricated using PDMS and have a semi-two-dimensional structure. The networks consist of square pores with the side length of $l=1$ mm and of rectangular throats with a randomly distributed width w. The ducts, i.e., pores and throats, have the same depth of $h=0.1$ mm. The distance between the centers of two neighboring pores is $a=2$ mm.

Two types of networks with different throat width distributions are used. In the network of type A, the throat widths are uniformly distributed in the range [0.14–0.94] mm. The minimal difference between two throat widths is 0.02 mm so as to relieve the effects of the fabrication uncertainty (± 0.01 mm). In the network of type B, the throat widths are 0.86, 0.88, 0.90, or 0.92 mm. Both networks have a size of 4×4 throats. Fig. 1 shows the structures of these two networks, where the numbers are the throat widths (the unit is mm). The middle pore at one side of the network is connected to an inlet tube of 0.5 mm wide and of 8 mm long, through which the invading fluid is injected. Opposite to this inlet side is the outlet open to the environment. The other two sides are impermeable.

The network is initially filled with the displaced fluid (air). The invading fluid is then injected into the network until the breakthrough moment. In the drainage experiment, the invading fluid is water with an advancing contact angle of about 67°. In the imbibition experiment, the invading fluid is the mixture of 20% v/v water and 80% v/v alcohol with an advancing contact angle of about 103°. The contact angle is measured in the displaced fluid. Dye agents are not used in the invading fluids to avoid wettability changes and duct blockages. The network is placed horizontally on a base to eliminate the effects due to gravitational forces.

The invading fluid is injected into the network by using a syringe pump (Harvard Apparatus, 11 Plus, USA). The flow rate is controlled to 0.1 μl/min so as to achieve a low capillary number ($Ca\sim 10^{-8}$). The capillary number is defined as $Ca=\mu v/\sigma$, where σ is the surface tension, and μ and v are the viscosity and velocity of the invading fluid, respectively. The movement of the invading fluid is recorded by a camera equipped with a macro lens (Nikon D810, Japan).

3. Pore network model

During the immiscible two-phase flow in a network, the invading and displaced fluids are separated by menisci inside ducts, across which a pressure difference is established:

$$\Delta P = P_{invading\ \ fluid} - P_{displaced\ \ fluid} = \sigma\left(\frac{1}{r_w}+\frac{1}{r_h}\right) \tag{1}$$

where r_w and r_h are radii of curvatures of menisci in the width and height directions, respectively. These two curvature radii are vector quantities and have direction as well as magnitude. A curvature radius is taken as positive if the center is at the side of the invading fluid, otherwise negative. The network ducts have the same height but various widths. Hence, r_w varies from ducts to ducts; r_h remains constant and equals to $r_h=h/2\cos\theta_a$, where θ_a is the advancing contact angle. For this reason, only the variation of r_w is investigated in the following analysis.

For a meniscus in a duct of width w, its curvature radius is $r_w=w/2\cos\theta$, where θ is the contact angle taken in the displaced fluid. The pressure difference across the meniscus increases with decreasing θ, Eq. (1). The three-phase contact line, where the invading fluid, displaced fluid, and solid meet, cannot move forward if $\theta>\theta_a$. Hence, to advance the meniscus, the pressure difference across it must exceed that at $\theta=\theta_a$. This critical value is called the threshold pressure (Lenormand et al., 1983). The

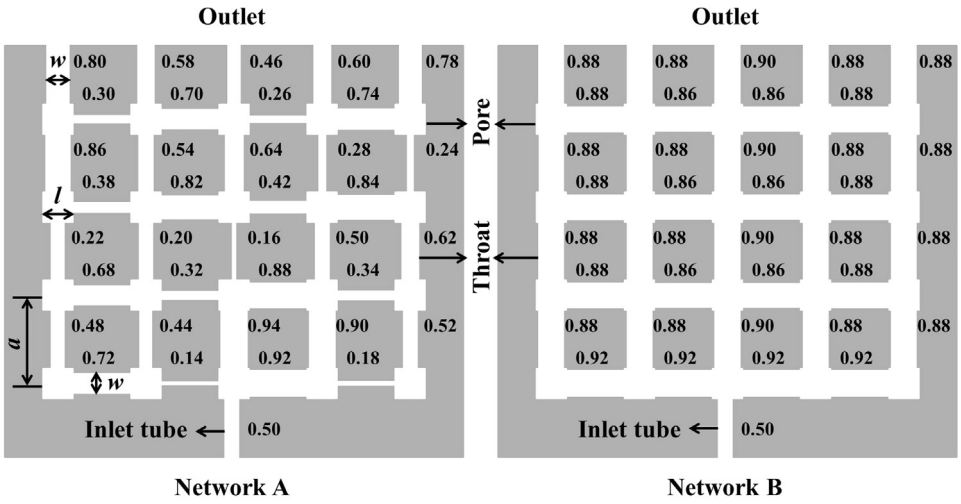

Fig. 1. Structures of the networks used in this work. The numbers are throat widths (the unit is mm).

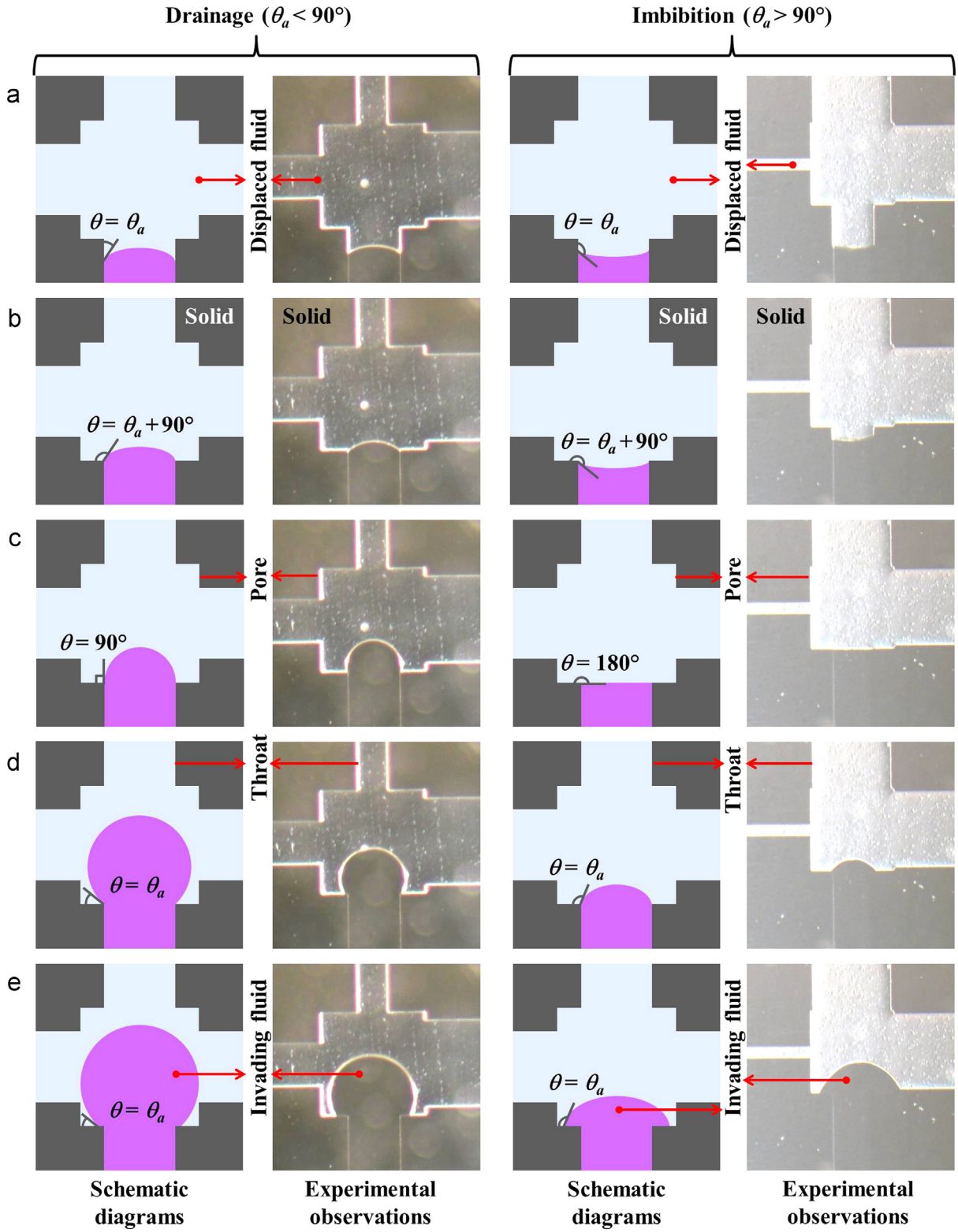

Fig. 2. Schematic and experimental observation of bursting invasion into a pore: (a) advancement of the three-phase contact line in the throat; (b–d) evolution of the meniscus when the three-phase contact line is pinned at the throat-pore interface; (e) advancement of the three-phase contact line along the pore wall.

threshold pressure of a throat with width w and height h is:

$$P_t = 2\cos\theta_a\sigma\left(\frac{1}{w}+\frac{1}{h}\right) \tag{2}$$

Fig. 2 shows how the invading fluid enters a pore from one throat. This type of pore invasion is called bursting invasion. The contact angle jumps to $\theta=\theta_a+90°$ when the three-phase contact line reaches the throat-pore interface, Fig. 2(a) and (b). The three-phase contact line then remains pinned. The curvature radius is $r_w=w/2\sin\theta$, where w is the throat width. The contact angle reduces from $\theta=\theta_a+90°$ to θ_a as the meniscus grows, Fig. 2(b)–(d). During this period, the pressure difference across the meniscus

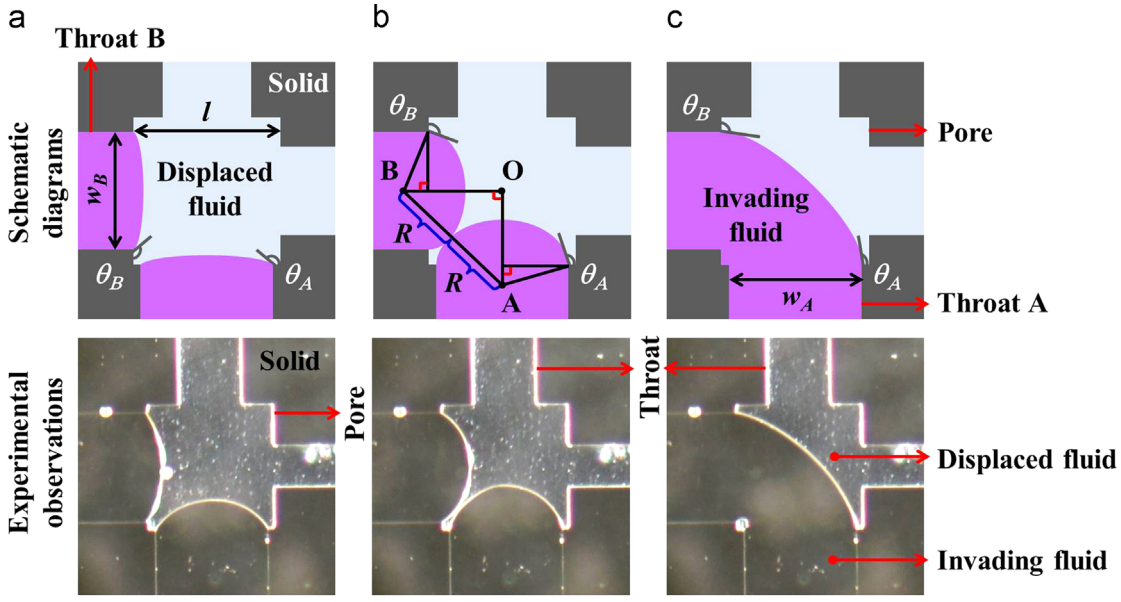

Fig. 3. Schematic and experimental observation of merging invasion into a pore: (a) before touching of two menisci; (b) at the moment of touching; (c) after touching of two menisci.

is largest at $\theta=\max(90°, \theta_a)$, i.e., 90° in drainage and θ_a ($>90°$) in imbibition. The three-phase contact line advances along the pore wall as θ reaches θ_a, Fig. 2(d) and (e). The curvature radius then increases, resulting in a lower pressure difference across the meniscus, Eq. (1). Hence, the threshold pressure for bursting invasion into a pore is:

$$P_t = 2\sigma\left(\frac{\sin\,[\max(90^\circ,\theta_a)]}{w}+\frac{\cos\,\theta_a}{h}\right) \tag{3}$$

where w and h are the throat width and height, respectively.

Owing to the sudden geometrical expansion at the throat-pore interfaces, the threshold pressure to invade a throat is smaller than that to burst from it into a pore, Eqs. (2) and (3). This is called the capillary valve effect. During the two-phase flow in a network, a meniscus will stop moving when it reaches the entrance of a pore. The pressure of the invading fluid then increases, which can cause the advancement of other menisci. As a result, two or more throats adjacent to a pore can be invaded before invasion into this pore.

Fig. 3 shows how the invading fluid enters a pore from two throats. Throats A and B are invaded, and $w_A > w_B$. Menisci A and B have the same curvature radii since the pressure differences across them are identical when two-phase invasion is dominated by capillary forces. This also implies $\theta_A > \theta_B$. The menisci touch each other at $\theta_A > \max(90°, \theta_a)$. The curvature radii are $r_w = w_A/2\sin\theta_A$ before touching, Fig. 3(a) and (b). After touching, a new meniscus forms, leading to a larger r_w, Fig. 3(c). The pressure difference across the menisci is largest at the moment of touching, Eq. (1). This type of pore invasion is called merging invasion. The threshold pressure is:

$$P_t = \sigma\left(\frac{1}{R}+\frac{2\,\cos\,\theta_a}{h}\right) \tag{4}$$

where R is the curvature radius at the moment of menisci touching.

As elucidated in Fig. 3(b), the value of R can be determined by the relationship $AB^2 = OA^2 + OB^2$:

$$(2R)^2 = \left[\frac{l}{2}+\sqrt{R^2-\left(\frac{w_A}{2}\right)^2}\right]^2+\left[\frac{l}{2}+\sqrt{R^2-\left(\frac{w_B}{2}\right)^2}\right]^2 \tag{5}$$

At the moment of menisci touching, θ_A is larger than the value of $\max(90°, \theta_a)$, which implies:

$$R > \frac{w_A}{2\,\sin\,[\max(90^\circ,\theta_a)]} \tag{6}$$

The menisci cannot touch at $\theta_A \geq 145°$ since pores are square and larger than their adjacent throats. This means:

$$R < \frac{w_A}{\sqrt{2}} \tag{7}$$

The value of R can be gained from Eqs. (5)–(7). If no solution is found, merging invasion shown in Fig. 3 will not occur; and the pore will be invaded by bursting invasion from throat A.

If the menisci shown in Fig. 3 touched at $\theta_A \leq \max(90°, \theta_a)$, the pressure difference across the menisci would be largest at $\theta_A = \max(90°, \theta_a)$. This type of pore invasion is still called bursting invasion because the threshold pressure is equal to that for bursting invasion from throat A. The menisci shown in Fig. 3 are neighboring to each other. If they were opposite, merging invasion would not occur. Three or more menisci attached to a pore cannot touch simultaneously since throats have various sizes. As a result, only merging invasion by two neighboring menisci is considered.

The following procedure is used to check whether a pore is invaded by bursting or merging invasion. First, the invaded throats adjacent to the pore are determined, and the meniscus attached to the largest one is called meniscus A. The menisci neighboring to meniscus A are then scanned. If there is no such meniscus, the pore will be invading by bursting invasion. If there are menisci neighboring to meniscus A, the one attached to the throat of the largest size is identified and called meniscus B. Possibility of merging invasion by menisci A and B is then checked by Eqs. (5)–(7). Merging invasion will happen if a solution is found; otherwise bursting invasion will occur.

The following algorithm is applied to the capillary force dominated two-phase flow in a network. At each step, only the available duct with the lowest threshold pressure is invaded. A duct is trapped if it is filled with the displaced fluid, and there is no flow path between it and the outlet. A duct is available if it is filled with displaced fluid, not trapped, and adjacent to an invaded duct. The threshold pressure of an available duct is determined by

Eqs. (2)–(7). If the capillary valve effect is neglected, the threshold pressures of all available ducts will be computed by Eq. (2) with w being the duct width.

4. Results and discussion

Figs. 4–6 compare the numerical and experimental results for the two-phase flows in the networks of types A and B. The numerical results are obtained from the pore network model with the capillary valve effect. In the images for the numerical results, the invaded throats are red; the pores invaded by bursting and merging invasion are blue and yellow, respectively; the ducts full of the displaced fluid are white; and the solid is gray. In the images for the experimental results, the invading fluid is black; the displaced fluid is white; and the solid is gray. The raw experimental images are presented in the Supplementary material.

As can be seen from Figs. 4–6, the numerical results agree well with the experimental observations. This validates the effectiveness of the pore network model developed in the present work.

For two-phase flows in the network of type A, pore invasion is dominated by bursting invasion, Figs. 4 and 5. Drainage and imbibition are similar. The only difference is that more throats are invaded in imbibition. In this case, throats have a lower threshold

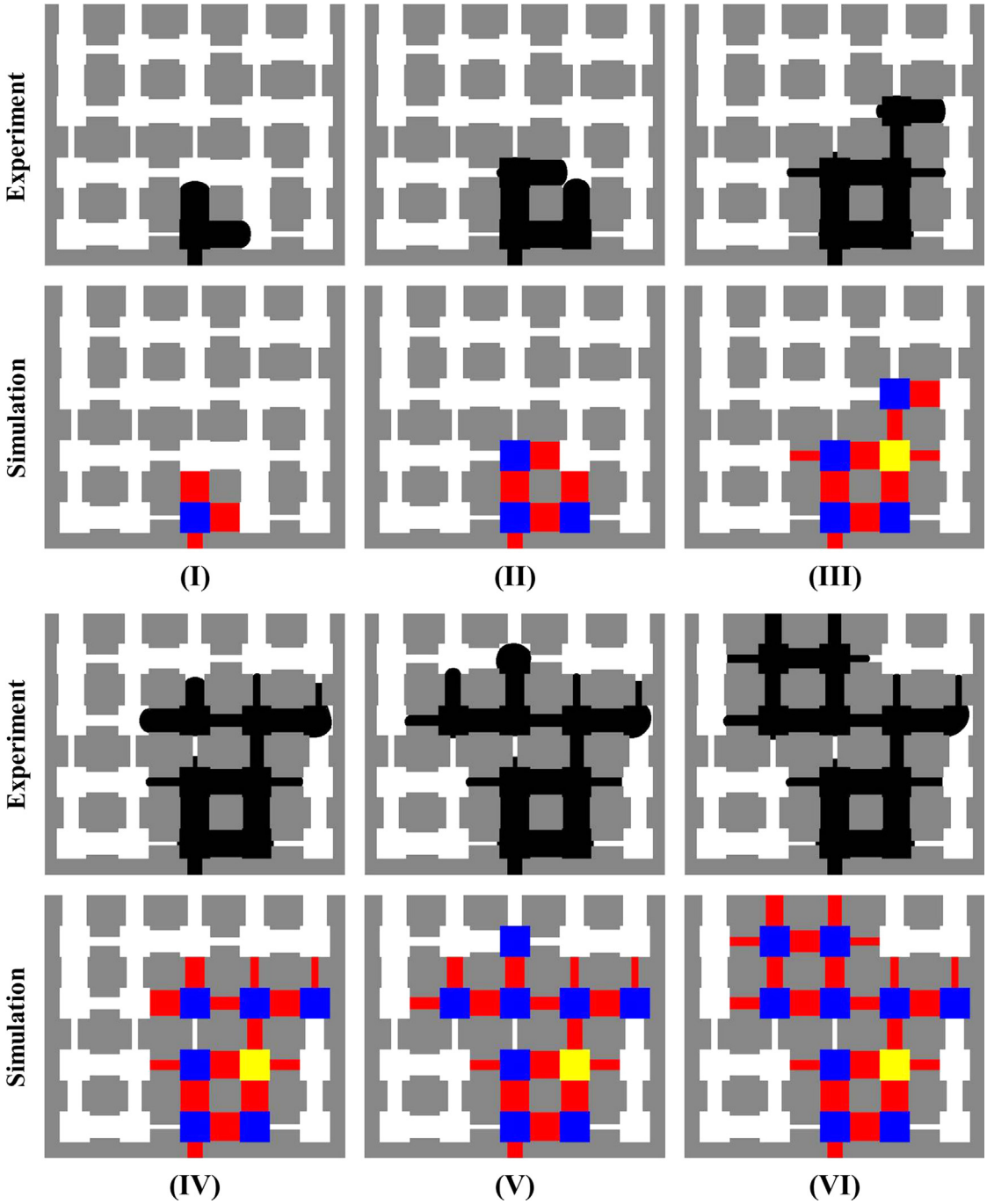

Fig. 4. Comparison between drainage in the network of type A obtained from the experiments and the pore network model with the capillary valve effect. Stage VI is the breakthrough moment. In the images for the numerical results, the invaded throats are red; the pores invaded by bursting and merging invasion are blue and yellow, respectively; the ducts filled with the displaced fluid are white; and the solid is gray. In the images for the experimental results, the invading fluid is black; the displaced fluid is white; the solid is gray. (For interpretation of the references to color in this figure legend, the reader is referred to the web version of this article.)

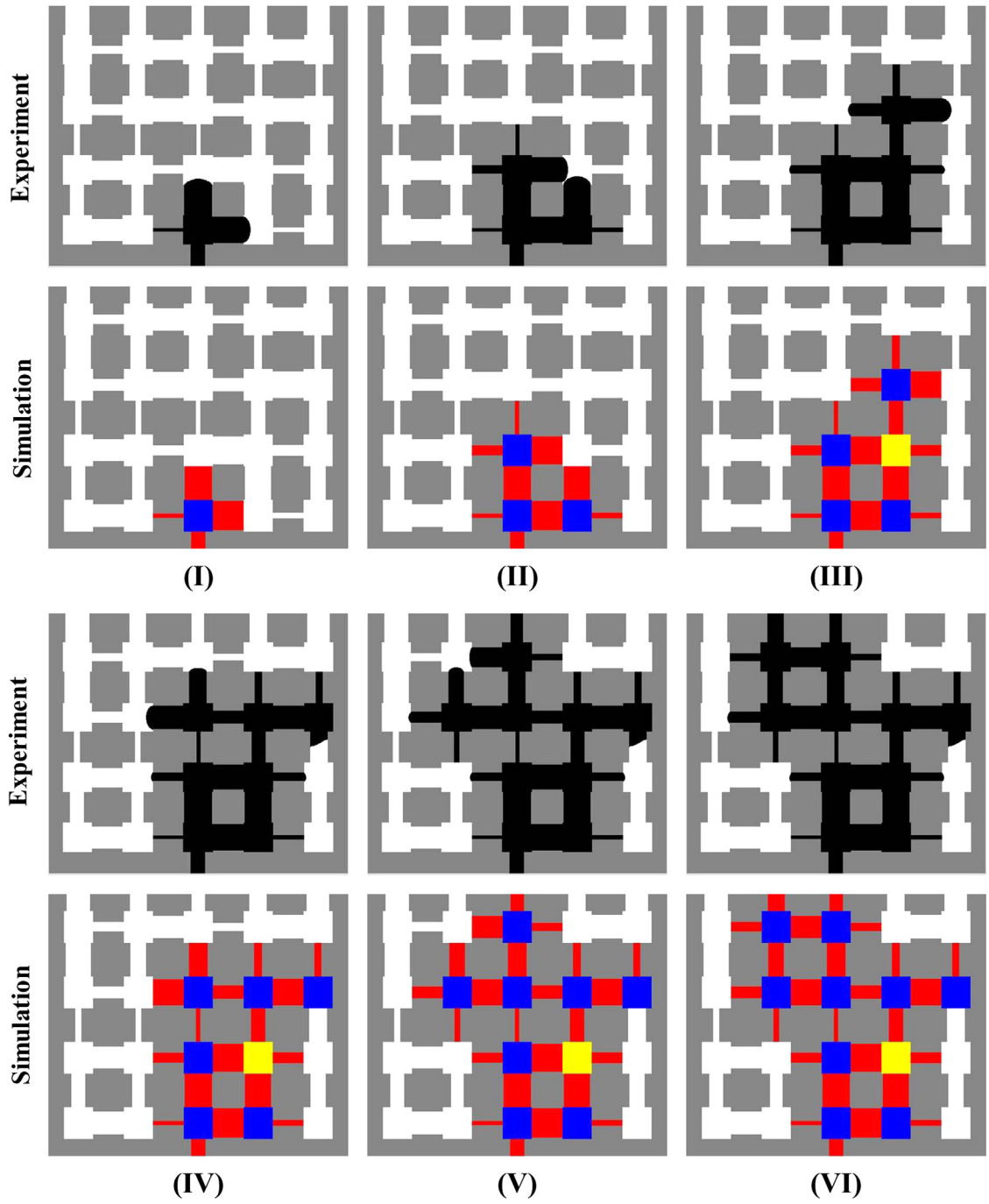

Fig. 5. Comparison between imbibition in the network of type A obtained from the experiments and the pore network model with the capillary valve effect. Stage VI is the breakthrough moment. The use of colors is same to that in Fig. 4. (For interpretation of the references to color in this figure legend, the reader is referred to the web version of this article.)

pressure than pores; and all available throats are invaded before next pore invasion. In drainage, an available throat is invaded before next pore invasion if it is greater than the largest invaded throat connected to an available pore.

Both drainage and imbibition show the following invasion characteristics. Before pore invasion, the invading fluid has occupied the largest throat between an invaded pore and a non-trapped pore full of the displaced fluid; the available pore connected to this largest invaded throat will be invaded in next pore invasion. As a result, drainage and imbibition in the network of type A are similar and exhibit a capillary fingering pattern, Figs. 4 and 5.

For drainage in the network of type B, pore invasion is dominated by merging invasion, Fig. 6. In this case, the ducts have similar sizes; and the invasion processes are affected significantly by the fabrication uncertainty. Differences in the invasion order are found between the simulation and the experiment, e.g., invasion into the left down pore. The experimental results are expected to be the same as the numerical results if the fabrication uncertainty is reduced. For this reason, we focus on the numerical results in the following analysis.

The network is divided into four layers from the inlet to the outlet. Each layer has five pores and four throats. The throats in the first layer are larger than others, Fig. 1. Hence this layer is invaded

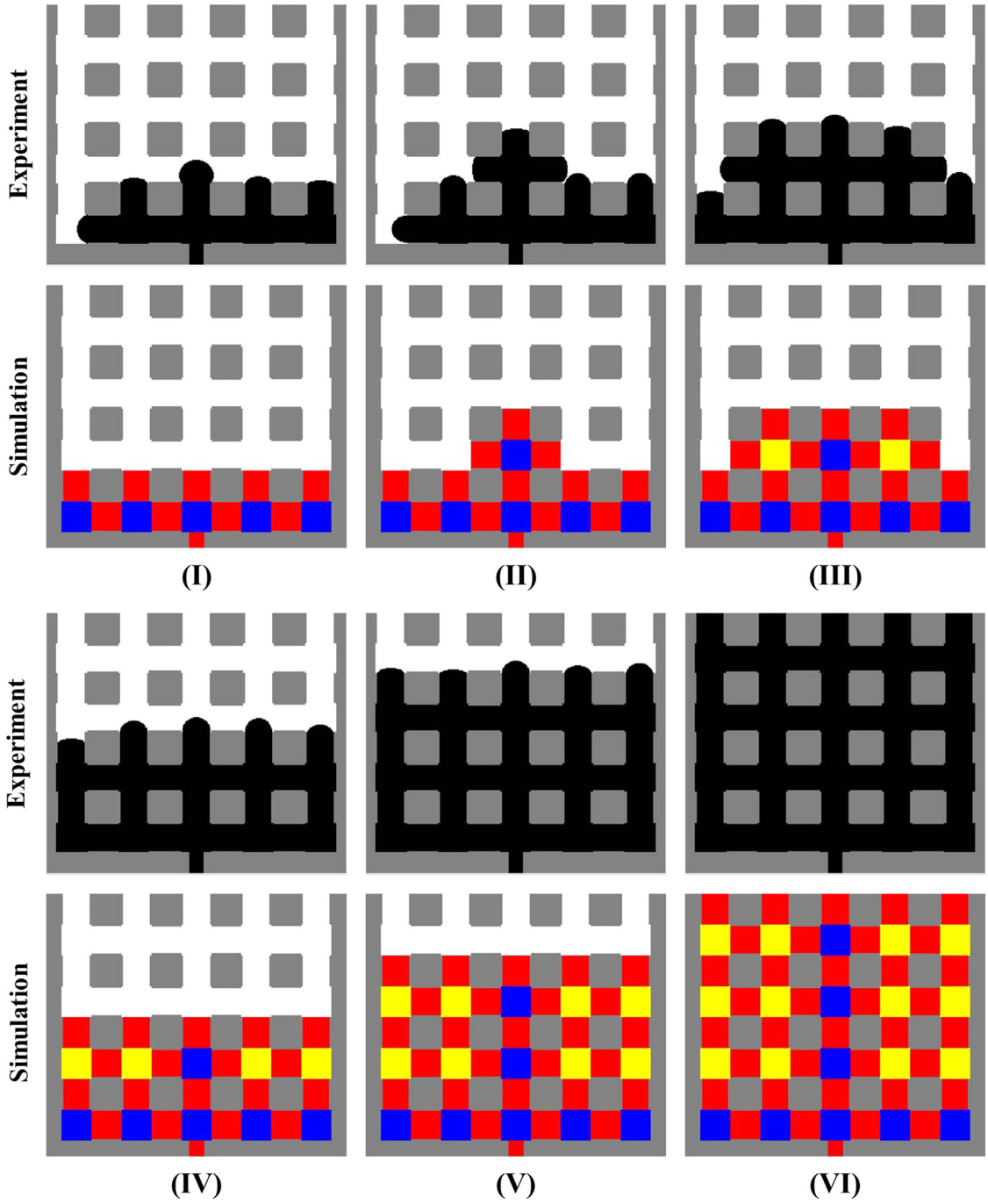

Fig. 6. Comparison between drainage in the network of type B obtained from the experiments and the pore network model with the capillary valve effect. Stage VI is the breakthrough moment. The use of colors is same to that in Fig. 4. (For interpretation of the references to color in this figure legend, the reader is referred to the web version of this article.)

first. This resembles invasion from an open face of the network. All throats between the first and second layers are invaded before invasion into a pore in the second layer, Fig. 6(I). This is because threshold pressures for bursting invasion into pores are larger than those of throats.

A pore in the network of type B will be invaded by merging invasion if two neighboring menisci are attached to this pore. Merging invasion has a lower threshold pressure than bursting invasion. Hence, after the invading fluid occupies a pore in the second layer and its connected throats, the available pores in the second layer adjacent to this invaded pore are invaded in the next step, Fig. 6(II) and (III). Pore invasion in the third layer will not happen unless all the pores in the second layer are invaded, Fig. 6 (IV). Invasion in the left network layers follows a similar way, Fig. 6 (V) and (VI). Thus, a stable invasion pattern is observed.

Lenormand (1990) has revealed that slow drainage in a porous medium is a capillary fingering pattern. This study, however, shows that the stable pattern is also possible, Fig. 6.

Fig. 7 shows the phase distributions at the breakthrough moment predicted by the pore network model without the capillary valve effect. The numerical and experimental results are similar for drainage in the network of type A, Figs. 4(VI) and 7(a).

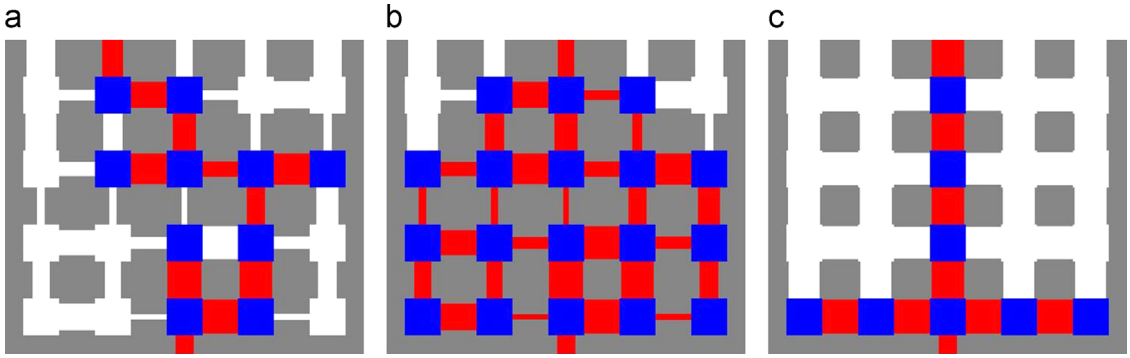

Fig. 7. Phase distributions at the breakthrough moment obtained from the pore network model without the capillary valve effect: (a) drainage in the network type A; (b) imbibition in the network of type A; (c) drainage in the network of type B. The invaded throats and pores are red and blue, respectively; the ducts filled with the displaced fluid are white; and the solid is gray. (For interpretation of the references to color in this figure legend, the reader is referred to the web version of this article.)

They are quite different for imbibition in the network of type A, Figs. 5(VI) and 7(b). The huge difference is also observed for drainage in the network of type B, Figs. 5(VI) and 7(c).

5. Conclusions

The capillary valve effect is studied for the capillary forced dominated immiscible two-phase flows in the networks composed of regular pores and throats. Two types of networks are used. In the network of type A, the throat widths are distributed from 0.14 to 0.94 mm. In the network of type B, the throat widths are distributed from 0.86 to 0.92 mm. All the pores have the same side length of 1 mm. Gas–liquid two-phase flows in these two networks are visualized experimentally. Two types of pore invasion are revealed. One is bursting invasion, where the invading fluid enters a pore from one throat. The other is merging invasion, where a pore is invaded by the invading fluid from two throats.

A pore network model is developed to include the capillary valve effect. The numerical results agree well with the experimental data. For drainage and imbibition in the network of type A, pore invasion is dominated by bursting invasion, and the flow pattern is capillary fingering. Drainage and imbibition in this network are similar; the only difference is that more throats are invaded in imbibition. For drainage in the network of type B, pore invasion is dominated by merging invasion, and the flow pattern is stable.

The results obtained from the pore network model without the capillary effect are also compared with the experimental data. The numerical and experimental results are similar for drainage in the network of type A. But they are quite different for imbibition in the network of type A as well as for drainage in the network of type B. The results presented in this work show clearly that the capillary valve effect needs to be considered to understand in detail the two-phase flows in porous media.

Acknowledgment

The first author is grateful for support of the National Natural Science Foundation of China (No. 51306124), the Natural Science Foundation of Shanghai City (No. 13ZR1458300), and the Alexander von Humboldt Foundation.

Appendix A. Supplementary material

Supplementary data associated with this article can be found in the online version at http://dx.doi.org/10.1016/j.ces.2015.09.028.

References

Araujo, A.D., Vasconcelos, T.F., Moreira, A.A., Lucena, L.S., Andrade, J.S., 2005. Invasion percolation between two sites. Phys. Rev. E 72, 041404.
Bazylak, A., Berejnov, V., Markicevic, B., Djilali, S.N., 2008. Numerical and microfluidic pore networks: towards designs for directed water transport in GDLs. Electrochim. Atca 53, 7630–7637.
Blunt, M., 2001. Flow in porous media – pore-network models and multiphase flow. Curr. Opin. Colloid Interface Sci. 6, 197–207.
Blunt, M., King, M.J., Scher, H., 1992. Simulation and theory of two-phase flow in porous media. Phys. Rev. A 46, 7680–7699.
Ceballos, L., Prat, M., Duru, P., 2011. Slow invasion of a nonwetting fluid from multiple inlet sources in a thin porous layer. Phys. Rev. E 84, 056311.
Ceballos, L., Prat, M., 2013. Slow invasion of a fluid from multiple inlet sources in a thin porous layer: influence of trapping and wettability. Phys. Rev. E 87, 043005.
Chapuis, O., Prat, M., Quintard, M., Chane-Kane, E., Guillot, O., Mayer, N., 2008. Two-phase flow and evaporation in model fibrous media: application to the gas diffusion layer of PEM fuel cells. J. Power Sources 178, 258–268.
Chen, J.M., Huang, P.C., Lin, M.G., 2008. Analysis and experiment of capillary valve for microfluidics on a rotating disk. Microfluid. Nanofluid. 4, 427–437.
Cho, H., Kim, H.Y., Kang, J.Y., Kim, T.S., 2007. How the capillary burst microvalve works. J. Colloid Interface Sci. 306, 379–385.
Duffy, D.C., Gillis, H.L., Sheppard, N.F., Kellogg, G.J., 1999. Microfabricated centrifugal microfluidic systems: Characterization and multiple enzymatic assays. Anal. Chem. 71, 4669–4678.
Joekar-Niasar, V., Hassanizadeh, S.M., 2012. Analysis of fundamentals of two-phase flow in porous media using dynamic pore network models: a review. Crit. Rev. Env. Sci. Technol. 42, 1895–1976.
Knackstedt, M.A., Sheppard, A.P., Pinczewski, W.V., 1998. Simulation of mercury porosimetry on correlated grids: evidence for extended correlated heterogeneity at the pore scale in rocks. Phys. Rev. E 58, R6923–R6926.
Knackstedt, M.A., Sheppard, A.P., Sahimi, M., 2001. Pore network modelling of two-phase flow in porous rock: the effect of correlated heterogeneity. Adv. Water Resour. 24, 257–277.
Lenormand, R., 1990. Liquids in porous media. J. Phys.: Condens. Matter 2, SA79–SA88.
Lenormand, R., Zarcone, C., Sarr, A., 1983. Mechanisms of the displacement of one fluid by another in a network of capillary ducts. J. Fluid Mech. 135, 337–353.
Lopez, R.H., Vidales, A.M., Zgrablich, G., 2003. Fractal properties of correlated invasion percolation patterns. Phys. A 327, 76–81.
Mani, V., Mohanty, M.M., 1999. Effect of pore space spatial correlations on two-phase flow in porous media. J. Petrol. Sci. Eng. 23, 173–188.
Moore, J.L., Cuiston, A.M., Mittendorf, I., Ottway, R., Johnson, R.D., 2011. Behavior of capillary valves in centrifugal microfluidic devices prepared by three-dimensional printing. Microfluid. Nanofluid. 10, 877–888.
Rebai, M., Prat, M., 2009. Scale effect and two-phase flow in a thin hydrophobic porous layer. Application to water transport in gas diffusion layers of proton exchange membrane fuel cells. J. Power Sources 192, 534–543.
Sahimi, M., 2011. Flow and Transport in Porous Media and Fractured Rock: From Classical Methods to Modern Applications, second edition. WILEY-VCH, Germany.
Wilkiinson, D., Willemsen, J.F., 1983. Invasion percolation: a new form of percolation theory. J. Phys. A: Match. Gen. 16, 3365–3376.
Wu, R., Liao, Q., Zhu, X., Wang, H., 2010. Determination of oxygen effective diffusivity in porous gas diffusion layer using a three dimensional pore network model. Electrochim. Atca 53, 7394–7403.
Wu, R., Liao, Q., Zhu, X., Wang, H., 2012. Liquid and oxygen transport through bilayer gas diffusion materials of proton exchange membrane fuel cells. Int. J. Heat Mass Tran. 55, 6363–6373.
Wu, R., Zhu, X., Liao, Q., Chen, R., Cui, G.M., 2013. Liquid and oxygen transport in defective bilayer gas diffusion material of proton exchange membrane fuel cell. Int. J. Hydrog. Energy 38, 4067–4078.